Bioorganometallic mechanism of action, and inhibition, of IspH

Weixue Wang[a], Ke Wang[b], Yi-Liang Liu[a], Joo-Hwan No[a], Jikun Li[a], Mark J. Nilges[c], and Eric Oldfield[a,b,1]

[a]Center for Biophysics and Computational Biology, University of Illinois, Urbana, IL 61801; [b]Department of Chemistry, University of Illinois, 600 South Mathews Avenue, Urbana, IL 61801; [c]Illinois EPR Research Center, 506 South Mathews Avenue, Urbana, IL 61801

Edited* by Jack Halpern, The University of Chicago, Chicago, IL, and approved December 29, 2009 (received for review September 25, 2009)

We have investigated the mechanism of action of *Aquifex aeolicus* IspH [E-4-hydroxy-3-methyl-but-2-enyl diphosphate (HMBPP) reductase], together with its inhibition, using a combination of site-directed mutagenesis (K_M, V_{max}), EPR and ^{1}H, ^{2}H, ^{13}C, ^{31}P, and ^{57}Fe-electron-nuclear double resonance (ENDOR) spectroscopy. On addition of HMBPP to an (unreactive) E126A IspH mutant, a reaction intermediate forms that has a very similar EPR spectrum to those seen previously with the HMBPP "parent" molecules, ethylene and allyl alcohol, bound to a nitrogenase FeMo cofactor. The EPR spectrum is broadened on ^{57}Fe labeling and there is no evidence for the formation of allyl radicals. When combined with ENDOR spectroscopy, the results indicate formation of an organometallic species with HMBPP, a π/σ "metallacycle" or η^2-alkenyl complex. The complex is poised to interact with H^+ from E126 (and H124) in reduced wt IspH, resulting in loss of water and formation of an η^1-allyl complex. After reduction, this forms an η^3-allyl π-complex (i.e. containing an allyl anion) that on protonation (at C2 or C4) results in product formation. We find that alkyne diphosphates (such as propargyl diphosphate) are potent IspH inhibitors and likewise form metallacycle complexes, as evidenced by ^{1}H, ^{2}H, and ^{13}C ENDOR, where hyperfine couplings of approximately 6 MHz for ^{13}C and 10 MHz for ^{1}H, are observed. Overall, the results are of broad general interest because they provide new insights into IspH catalysis and inhibition, involving organometallic species, and may be applicable to other Fe_4S_4-containing proteins, such as IspG.

enzyme inhibition | iron-sulfur protein | isoprenoid biosynthesis | nonmevalonate pathway

Enzymes that catalyze the formation of isoprenoids are of interest as drug targets. There are two main pathways involved in the early steps in isoprenoid biosynthesis: The mevalonate pathway found in animals and in pathogens such as *Staphylococcus aureus*, *Trypanosoma cruzi*, and *Leishmania spp.* (the causative agents of staph infections, Chagas' disease and the leishmaniases), and the nonmevalonate or Rohmer pathway found in most pathogenic bacteria, as well as in the malaria parasite, *Plasmodium falciparum* (1). Both pathways lead to formation of the C_5-isoprenoids isopentenyl diphosphate (IPP, **1**) and dimethylallyl diphosphate (DMAPP, **2**). In the later stages of isoprenoid biosynthesis, these C_5-compounds then form the farnesyl diphosphate (FPP) and geranylgeranyl diphosphate (GGPP) used in protein prenylation, sterol, and carotenoid biosynthesis. Understanding how the enzymes catalyzing these "downstream" events function has led to a better understanding of e.g. how FPP synthase (2) and GGPP synthase function, and can be inhibited (3); the discovery that bisphosphonates have potent antiparasitic activity (4); the clinical use of amiodarone (a squalene oxidase and oxidosqualene cyclase inhibitor) against Chagas' disease (5; 6) and leishmaniasis (7); anticancer agents that inhibit both FPPS and GGPPS (8); as well as the discovery that cholesterol lowering agents (squalene synthase inhibitors) can function as antivirulence agents, against *S. aureus* (9). However, there have been few compounds discovered that block the nonmevalonate pathway, fosmidomycin being the notable exception (10). In this article, we focus on the last enzyme in the nonmevalonate pathway, IspH (LytB), with the goal of obtaining a better understanding of its mechanism of action, and inhibition.

The IspH (LytB) enzyme HMBPP (E-4-hydroxy-3-methyl-but-2-enyl diphosphate) reductase (EC 1.17.1.2) catalyzes the $2H^+/2e^-$ reduction of HMBPP (**3**) to form an approximately 5:1 mixture of IPP and DMAPP:

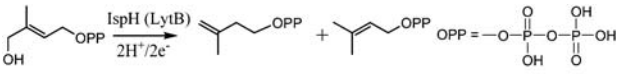

3 1 2

The enzyme is essential for survival and is not found in humans, so is an attractive target for drug development (11). The structures of IspH from *Aquifex aeolicus* (12) and *Escherichia coli* (13) have recently been reported and indicate trefoil-like protein structures with a central Fe_3S_4 cluster (14), whereas EPR (15), Mössbauer (16, 17), reconstitution and catalytic activity (15, 17) measurements have all been interpreted as indicating that an Fe_4S_4 cluster is the catalytically active species. Ligand-free IspH has an "open" structure (12), whereas IspH cocrystallized with diphosphate has a "closed" structure (13) in which a serine-X-asparagine (SXN) loop is involved in hydrogen bonding with a PPi ligand. The mechanism of action of IspH is controversial and there have been many different proposals (13, 15, 18–21) (Fig. S1). However, none of these models has yet been supported by any spectroscopic evidence, and none have led to the development of IspH inhibitors. Here, we report spectroscopic results that indicate the involvement in catalysis of π/σ metallacycle intermediates similar to those found for ethylene and allyl alcohol when bound to a nitrogenase FeMo cofactor (22–24). Then, based on these results, we show that *alkynes* can inhibit IspH, forming once again, metallacyles or π/σ complexes.

Results and Discussion

The Role of Protein Residues. We first investigated the role of protein residues in the IspH mechanism. In previous work, we noted that in addition to E126, His42, and His124 were also totally conserved residues, were located in the active site region, and were likely essential for catalytic activity, a conclusion now supported by mutagenesis results (13). However, the exact role of these residues was unclear. We thus determined the K_M and V_{max} values for three mutants: H42A, H124A, and E126A. In the case of the E126A mutant, activity was so low (V_{max} < 0.025 μmol min^{-1} mg^{-1}) that K_M could not be measured. But with the H124A mutant, we found that although V_{max} was low (0.05 μmol min^{-1} mg^{-1} versus 1.16 μmol min^{-1} mg^{-1} for the wild-type enzyme), K_M was essentially unchanged (7 μM versus

Author contributions: W.W., K.W., and E.O. designed research; W.W., K.W., Y.-L.L., J.-H.N., J.L., M.J.N., and E.O. performed research; W.W., J.-H.N., and E.O. analyzed data; K.W. and J.L. contributed new reagents/analytic tools; and E.O. wrote the paper.

The authors declare no conflict of interest.

This Direct Submission article had a prearranged editor.

[1]To whom correspondence may be addressed. E-mail: eo@chad.scs.uiuc.edu.

This article contains supporting information online at www.pnas.org/cgi/content/full/0911087107/DCSupplemental.

www.pnas.org/cgi/doi/10.1073/pnas.0911087107

5 μM, for the wild-type enzyme). This indicates that H124 is not a major contributor to substrate binding, but is essential for catalysis, suggesting that H124 may be involved in delivering H^+ to E126 and the bound HMBPP. In the case of H42, however, we find in the H42A mutant that there is an increase in K_M (from 7–74 μM), indicating a role in substrate binding, consistent with the crystallographic observation that H42 hydrogen bonds to a bound diphosphate ligand (13). There is, nevertheless, also a 5-fold decrease in V_{max}, due perhaps to the possibility that several more distal residues could also be involved in proton transfer.

EPR of IspH with Bound Ligands. As shown by Wolff et. al. (15), as-isolated, oxidized IspH (from *E. coli*) has low activity and exhibits an EPR spectrum characteristic of an $S = 1/2$ $[Fe_3S_4]^+$ cluster. On reconstitution (with DTT, Fe^{3+} and S^{2-}) and under reducing (excess dithionite) conditions, a broad, $S = 1/2$ EPR spectrum characteristic of an $[Fe_4S_4]^+$ cluster is obtained (15), essentially identical to that we find for reduced *A. aeolicus* IspH (Fig. 1*A*). On addition of HMBPP, the spectrum sharpens and several components can be seen (Fig. 1*B*). This suggests that HMBPP might bind to the cluster, or that HMBPP reacts and that the IPP/DMAPP products bind to the cluster, or that both occur. The observation that the IPP product can bind is supported by the observation that the spectrum of reduced, wild-type IspH plus IPP (Fig. 1*C*) is similar to that of the HMBPP spectrum. Clearly, this apparent reactivity complicates any determination of the details of HMBPP binding, so we next investigated the binding of HMBPP to the E126A mutant of IspH. In our previous work (12) we proposed that E126 was a key catalytic residue, a suggestion now confirmed by mutagenesis results (13). If E126 is inactivated by mutagenesis (to Ala), this should block catalysis, and might enable observation of an early reaction intermediate. As shown in Fig. 1*D*, the spectrum of the reduced E126A mutant + HMBPP is in fact now quite different to that seen with the wild-type enzyme + HMBPP, confirming this idea. The spectrum is broadened in an ^{57}Fe-labeled sample (Fig. S2*C*), indicating an $[Fe_4S_4]^+$rather than an organic radical, origin. Moreover, the *g*-values ($g = 2.124, 1.999, 1.958$, by simulation) are, interestingly, quite similar to those seen previously with ethylene and allyl alcohol bound to the α-70^{Ala} mutant of a nitrogenase FeMo cofactor protein [ethylene: $g = 2.123, 1.978, 1.949$ (24); allyl alcohol: $g = 2.123, 1.998, 1.986$ (22)] with, on average, only a $|0.01|$ difference between the IspH and nitrogenase *g*-values. In nitrogenase, ethylene and allyl alcohol have been shown [via ENDOR and/or density functional theory calculations (22–24)] to bind as π/σ "metallacycles," as shown e.g. in Fig. 1*E*. And because HMBPP is simply a substituted alkene, one possible explanation of the E126A + HMBPP spectrum is that HMBPP binds to reduced IspH in a similar manner, that is, as a π or π/σ "metallacycle" or "η^2-alkenyl" complex, similar to that shown in Fig. 1*F* (which is based on the nitrogenase/allyl alcohol structure and contains Mo and "X"). That such a complex could form with HMBPP is supported by the results of ligand docking calculations using Glide (25) (Fig. 1*G* and *H*) in which it can be seen that HMBPP can bind with its diphosphate occupying the "PPi" site seen crystallographically, at the same time that its double bond interacts with the unique fourth Fe, added computationally here as described previously (12). Based on the observation that only reduced Fe_4S_4 clusters bind alkynes (26), it seemed likely that only the reduced IspH would bind HMBPP in this manner, and to investigate this binding question in more detail, we used ENDOR to probe the HMBPP- reduced IspH interaction in more detail.

^{2}H, ^{13}C, ^{31}P, and ^{57}Fe ENDOR of IspH + Alkene Ligands. A test of this π/σ metallacycle complex formation hypothesis with reduced IspH is that there should be significant hyperfine couplings (A) with the ligand if it indeed bonds to the $S = 1/2$, $[Fe_4S_4]^+$ cluster. We thus prepared the following series of ^{2}H and ^{13}C isotopically labeled HMBPPs (**4**–**6**), and investigated their ENDOR spectra when bound to IspH.

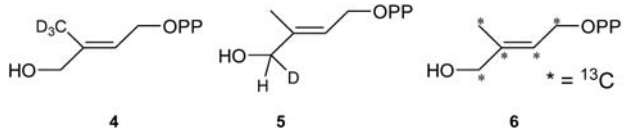

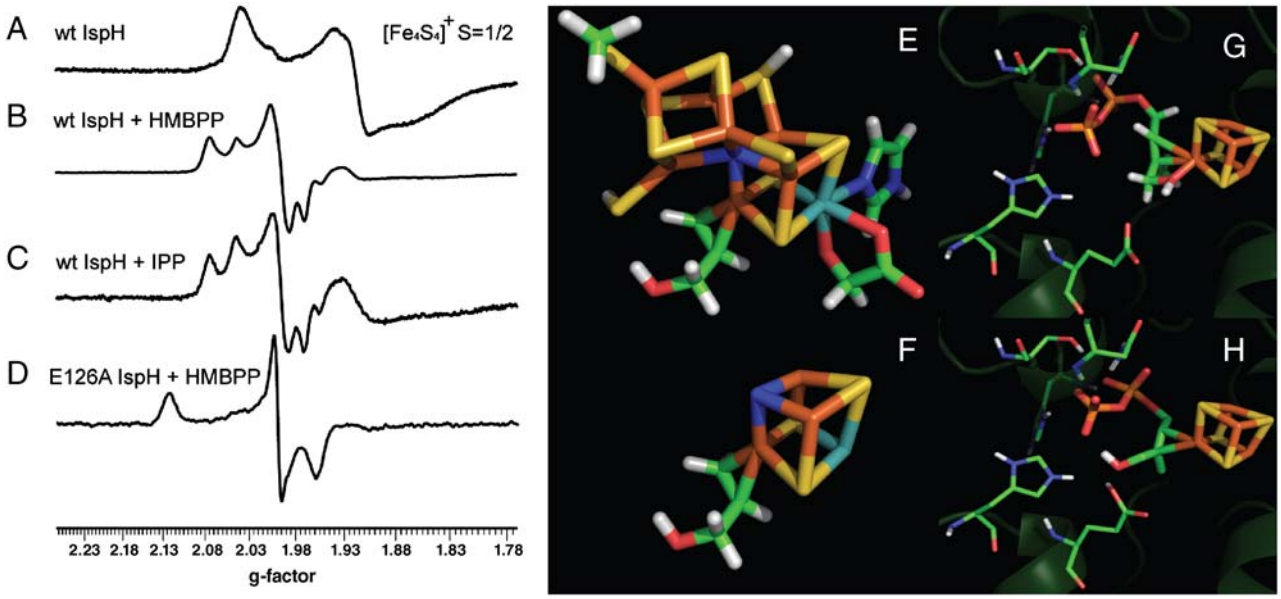

Fig. 1. 9 GHz EPR of *A. aeolicus* IspH, and molecular models for ligand interactions. (*A*) Wild-type IspH. (*B*) Wild-type IspH + HMBPP. (*C*) Wild-type IspH + IPP. (*D*) E126A IspH + HMBPP. Spectra were all obtained on samples reduced with 20 equivalents sodium dithionite (see *SI Text* for more details), and are essentially identical to those obtained in samples prepared via photoreduction (e.g. Fig. S2*A* and *B*). Microwave power was 1 mW for A–C, and 0.1 mW for D. (*E*) Structure of nitrogenase Fe/Mo cofactor + allyl alcohol. (*F*) As (*E*) but edited to more clearly show the allyl alcohol binding site. Mo (*Cyan*); "X" (*Blue*). (*G*) Glide docking result for HMBPP docking to IspH active site region. (*H*) As (*G*) but after molecular mechanics optimization.

On binding **4** to E126A IspH, we clearly see (Fig. 2*A*, *Bottom Trace*) a low frequency feature in the Mims ENDOR (27) difference spectrum attributable to the methyl deuterons, characterized by $A \sim 0.4$ MHz. At higher frequency, there is a peak centered at the ^{31}P Larmor frequency, but with a very small (<0.1 MHz) hyperfine coupling, in the ENDOR spectra of both **3** and **4** with IspH (Fig. 2*A*, *Inset in Black*). Essentially the same results are found on binding of **5** (which contains a 4-$^{2}H_1$ group), inset in blue above the 5-$^{2}H_3$ spectra, with A again being approximately 0.4 MHz for ^{2}H and <0.1 MHz for ^{31}P. With [u-^{13}C] HMBPP, **6**, there are two major features (having $A = 1.70, 0.80$ MHz, Fig. 2*B*), which we attribute to the olefinic carbons, $^{13}C2, 3$. Signals from $^{13}C1$, 4 and 5 are not observed, due we believe to very small couplings. These EPR and ^{2}H, ^{13}C ENDOR results support the idea that HMBPP bound to reduced IspH forms a metallacycle (that is, a π or η^2-alkenyl σ-like complex), just as found with ethylene and allyl alcohol binding to the nitrogenase FeMo protein cofactor (22–24).

^{57}Fe ENDOR spectra of [^{57}Fe]-IspH ± **3** also support the idea that **3** may bind directly to the Fe_4S_4 cluster. The ^{57}Fe Davies ENDOR spectrum (27) ($\pi/2_{mw} = 12$ ns, nonselective pulse) of IspH in the absence of any added ligands is broad (Fig. 2*C*) and there are three major features present. On binding **3**, a sharper ENDOR spectrum is seen. Using selective ($\pi/2_{mw} = 48$ ns) pulses in a Davies ENDOR spectrum, features attributable to ^{1}H as well as ^{57}Fe are observed (Fig. 2*D*); with nonselective pulses ($\pi/2_{mw} = 12$ ns) only two major Fe features are apparent (Fig. 2*E*) and these features (as expected) are absent in a control ([^{56}Fe] IspH + **3**) spectrum (Fig. 2*F*). The difference spectrum (2E-2F) is shown in Fig. 2*G*. No additional small ^{57}Fe hyperfine couplings are observed, as confirmed by Mims ENDOR. These results show that there are major changes in the electronic structure of the reduced Fe_4S_4 cluster on HMBPP addition, and strongly support the idea that HMBPP binds chemically to the cluster. This in turn supports the idea that the hyperfine couplings seen in the $^{2}H/^{13}C$ ENDOR results are not solely due to a dipolar or through space interactions but rather, arise (at least in part) from through bond, Fermi contact couplings. So, the results of both EPR and ENDOR spectroscopy indicate π or π/σ complex formation with reduced IspH and HMBPP, leading to the catalytic mechanism proposal described in the following.

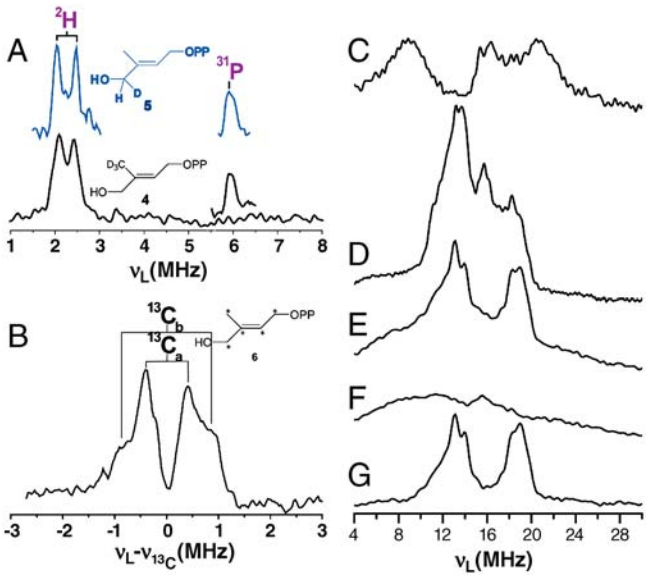

Fig. 2. ENDOR spectra of IspH with HMBPP. (*A*) E126A IspH + **4** (*Black*) or **5** (*Blue*). Spectra are difference spectra (^{2}H-^{1}H); the ^{31}P region is the unsubtracted ENDOR result. (*B*) E126A IspH + **6** minus E126A + **3**, showing solely ^{13}C ENDOR. (*C*) Unliganded wild-type [u-^{57}Fe]-IspH, with natural abundance ^{57}Fe control subtracted. (*D*) [u-^{57}Fe]-E126A IspH + HMBPP, ^{57}Fe ENDOR, Davies selective pulse. (*E*) As (*D*) but nonselective pulse. (*F*) As (*D*) but natural abundance ^{57}Fe-IspH. (*G*) Difference spectrum of (*E*) and (*F*).

Catalytic Mechanism of IspH. The models shown in Fig. 1*G* and *H* indicate that when the HMBPP diphosphate docks to the "PPi" site and the double bond forms a π/σ alkenyl complex with the (reduced) Fe_4S_4 cluster, the CO_2H group of E126 is approximately 2.3 Å from the HMBPP 4-OH group. This then suggests the catalytic mechanism shown in Fig. 3 in which: (*i*) After initially binding to the oxidized cluster via oxygen (Fig. 3*A*), on reduction a π (or π/σ) complex forms (Fig. 3*B* and *C*), "activating" the substrate for the subsequent deoxygenation. The structure shown in Fig. 3*B* is the π-complex, but the proposed reaction can arguably be better followed via the η^2-alkenyl/metallacycle, Fig. 3*C*. (*ii*) This reduced complex is then protonated via E126 (and H124A), resulting in formation of water and an η^1-allyl complex, Fig. 3*D*. (*iii*) After a second reduction, the η^3-allyl complex forms (Fig. 3*E* and *F*), with protonation at C2 or C4 then forming the two products, DMAPP and IPP (Fig. 3*G* and *H*). One potential drawback of this mechanism might be that the E126 carboxyl is not acidic enough to protonate the 4-OH. However, H124 is close by (approximately 5 Å from the H124 N^{δ} to E126 carboxyl oxygen, PDB file #3F7T), and could be involved in increasing the acidity of E126, either directly or via an intervening H_2O. The source of H^+ in the second part of reaction, the reductive cleavage, could be via E126 (in the case of DMAPP formation), or solvent (e.g. H_3O^+ in a "water" site), for IPP (because there are no other obvious H^+ donors apparent).

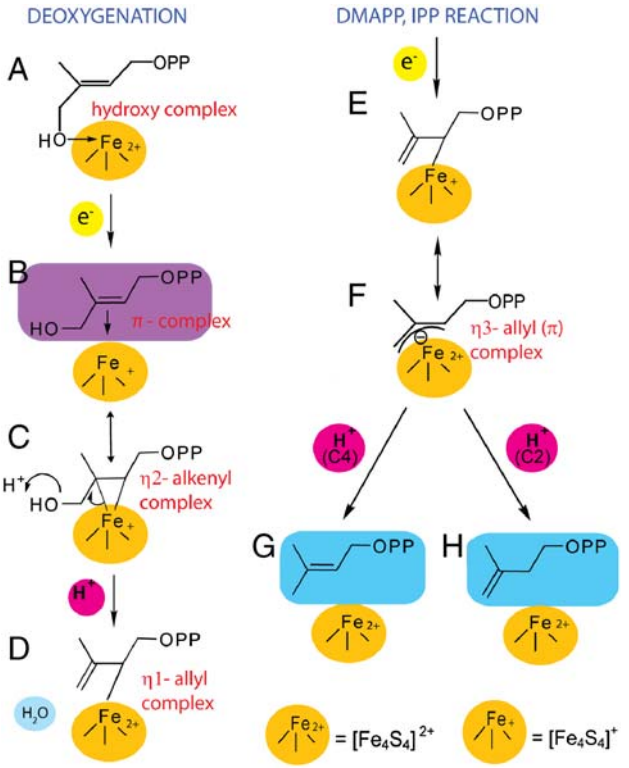

Fig. 3. Proposed mechanism of action of IspH. (*A*) Oxidized Fe_4S_4 cluster plus HMBPP (12); (*B*) the Fe_4S_4 cluster has been reduced by one electron; the structure is generally similar to that found for allyl alcohol bound to nitrogenase; (*C*) π/σ complex (shown for simplicity as the η^2-alkenyl metallacycle) is protonated by E126/H124A; (*D*) After protonation, the 4-OH is removed as H_2O, forming an η^1-allyl complex; (*E*) the Fe_4S_4 cluster is reduced by second e^-, and subsequently forms a η^3-allyl (π) complex, (*F*); (*G*) protonation at C4 results in DMAPP product; (*H*) IPP is formed by protonation at C2.

A simplified version of the mechanism, together with the locations of the reactants/intermediates/products in IspH is illustrated in Fig. 4. In Fig. 4*A*, we show a docking pose for HMBPP bound to reduced IspH (PDB file #3F7T; chosen because it contains a PPi ligand and adopts the "closed" conformation) in which the diphosphate hydrogen bonds to S225, N227, and H42 while the side-chain fits the pocket near the Fe_4S_4 cluster. Note of course that, based on the spectroscopic and activity results, we show an Fe_4S_4 (not an Fe_3S_4) cluster. The double bond in HMBPP forms a π (or π/σ) complex with the reduced Fe_4S_4 cluster, based on the ENDOR results. As is well known in organometallic chemistry, such complexes are typically neither completely π nor completely σ, as discussed by Pelmenschikov et al. (23), but for convenience in drawing reaction mechanisms, is shown as a σ (η^2-alkenyl) complex in Figs. 3 and 4. On protonation of the 4-OH by E126 (possibly involving H124 and H_2O), the η^1-allyl complex and water form, Fig. 4*B*. After the second reduction, the η^3-complex forms (Fig. 4*C*), which is then protonated to form the two products (Fig. 4*D*). Although radical transition states or reactive intermediates may also be involved, the EPR and ENDOR spectra we do observe are unlikely to arise from allyl radicals because (*i*) allyl radicals would have 2 or 3 partially resolved peaks around the free electron *g*-value; (*ii*) they would have very large [approximately 50 MHz (28)] ^{13}C hyperfine couplings; (*iii*) they would not broaden on ^{57}Fe-labeling; plus (*iv*), the E126A mutant is essentially unreactive. The model proposed is, attractive because it invokes well-established precedent for the formation of π-complexes between Fe_4S_4 clusters and unsaturated species (alkynes, cyclopentadienides) (26, 29); such complexes are seen with the "parents" ethylene and allyl alcohol bound to the nitrogenase FeMo cofactor; we observe hyperfine couplings with bound substrate; docking puts the double bond next to the unique Fe, and the 4-OH close to the putative H^+ donor, E126; and there is no evidence for any allyl radical intermediates.

The Metallacycle Model Leads to Novel Inhibitors. The binding of acetylene to simpler Fe_4S_4 clusters, forming π complexes, Fig. 5*A*, has been observed in model systems such as $[Fe_4S_4(SPh)_4]^{2-/3-}$ (26, 30), and diphenylacetylene (**7**) binds to $[Fe_4S_4(SPh)_4]^{2-}$ where it can be *cis*-hydrogenated by $NaBH_4$ (31). This leads to the idea that acetylenes might bind to, and thus inhibit, IspH. We thus next investigated the inhibition of IspH by propargyl alcohol, **8**:

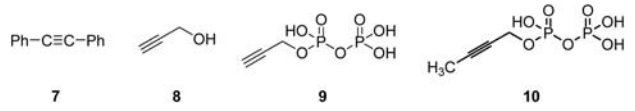

Inhibition was very low, $K_i > 10$ mM. On the other hand, propargyl diphosphate (**9**) was a more potent IspH inhibitor (Fig. 5*B*) with a $K_i = 0.97$ μM. This indicates that acetylenic diphosphates bind to IspH, most likely with their diphosphates occupying the "PPi" site, while their alkyne groups bind to the fourth Fe, forming a π/σ metallacycle. A docking pose for **9** bound to IspH is illustrated in Fig. 5*C* and clearly indicates that the alkyne is in close apposition with the fourth Fe, forming a metallacycle.

If such metallacycles form, it should be possible to investigate them spectroscopically. In particular, we expect to see major changes in the $[Fe_4S_4]^+$ EPR spectra, plus, ENDOR should indicate sizeable hyperfine couplings. The EPR spectra of IspH (+**8**, **9**, and **10**) are shown in Fig. 5*D–F* and indicate large *g*-value changes (from Fig. 1*A*) on ligand addition, suggesting an interaction with the Fe_4S_4 cluster. The Davies ^1H ENDOR spectrum (Fig. 6*A*) of IspH + **8** shows an approximately 10 MHz hyperfine coupling feature, while in the Davies ENDOR spectrum of IspH + [3-$^2H_1$]-**8**, the 10 MHz feature is greatly attenuated (Fig. 6*A*, *Inset*) and is replaced at low field by a 1.5 MHz hyperfine coupling feature in the ($^2H - ^1H$) difference Mims ENDOR spectrum (Fig. 6*B*), attributable to the 3-deuteron. The large ^1H and ^2H hyperfine couplings are similar to those seen in the nitrogenase system (22) and indicate formation of an organometallic species.

Additional evidence for formation of Fe-C bonds per se come from the results of ENDOR experiments using both [$^{13}C_3$]-**8** and [$^{13}C_3$]-**9** (Fig. 6*C* and *D*), where we see strong ^{13}C ENDOR peaks having quite large (6 MHz) hyperfine couplings. This, together with the docking result (Fig. 5*C*), suggests that both **8** and **9** bind to the Fe_4S_4 cluster at the fourth Fe, forming a π/σ complex, as with acetylene binding to model Fe_4S_4 clusters (26, 30). Also present in the ENDOR spectrum of **9** bound to IspH is a feature due to ^{31}P (Fig. 6*D* *Inset*, hyperfine coupling =0.3 MHz). We favor a sideways-on π-complex rather than the alternative end-on binding mode because (*i*) diphenylacetylene (**7**), which lacks a terminal H, binds to reduced Fe_4S_4 clusters (31) but as with acetylene (30), is still *cis*-reduced [by ^2H (31)]; (*ii*) the shift in the C ≡ C vibrational Raman spectrum (26) of C_2H_2 on binding to reduced Fe_4S_4 clusters is relatively small (approximately 60 cm^{-1}), whereas shifts seen on acetylide formation (or in mononuclear complexes) are typically 2–3x larger (32); (*iii*), compound **10**, which cannot bind end-on to IspH, still exhibits (Fig. 5*F*) a rhombic EPR spectrum similar to that seen with the terminal alkynes, Fig. 5*D* and *E*; and (*iv*), the observation of the ^2H ENDOR signal from the terminal ^2H in **8** is consistent with this binding mode: FeH would have a larger coupling, while SH would exchange away.

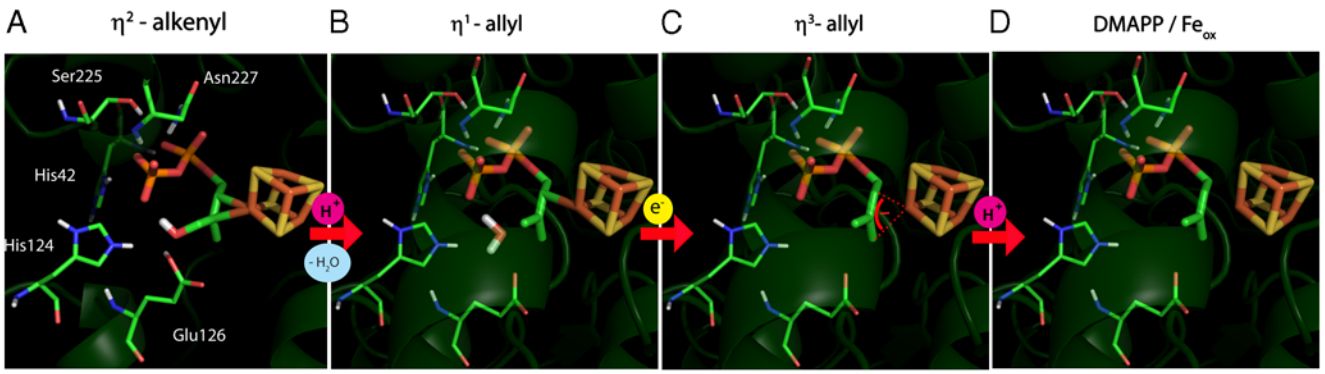

Fig. 4. Protein-based structural models for IspH catalysis. (*A*) HMBPP docks to the reduced active site with diphosphate binding to S225, N227, and H42, double bond forms π/σ complex with Fe_4S_4 cluster; (*B*) HMBPP 4-OH is protonated by E126, loss of H_2O results in η^1-allyl complex; (*C*) cluster is rereduced by one electron, forming an η^3-allyl (π) complex; (*D*) η^3-allyl complex is protonated at C4 forming DMAPP and oxidized cluster. Protonating the alternate η^3-allyl complex (or η^1-allyl species) at C2 results in IPP product formation (as in Fig. 3). Numbering is for the *A. aeolicus* protein.

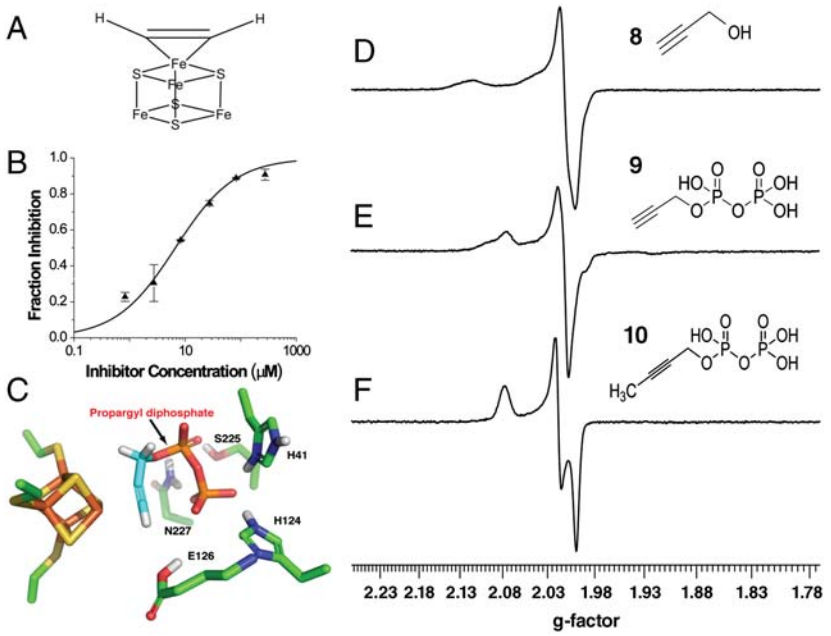

Fig. 5. Inhibition of IspH by alkynes. (*A*) Proposed binding mode of acetylene to an Fe_4S_4 cluster (26, 30). (*B*) IspH inhibition by **9**; $IC_{50} = 6.7$ μM; $K_i = 0.97$ μM. (*C*) Glide docking pose for **9** bound to IspH. The *E. coli* IspH structure (PDB 3F7T) and numbering are shown. (*D–F*) EPR spectra of three alkynes interacting with IspH: (*D*) **8**; (*E*) **9**; (*F*) **10**. Microwave power was 0.05 mW. All spectra show major *g*-value changes from those seen in the inhibitor-free protein, Fig. 1*A*.

The ^{57}Fe ENDOR spectra of [u-^{57}Fe]-IspH + **8** (and a ^{56}Fe control) are shown is Fig. 6*E–G*. The Davies selective pulse spectrum ($\pi/2_{mw} = 48$ ns, Fig. 6*E*) has both ^{1}H and ^{57}Fe contributions. The ^{1}H signal is edited out by using nonselective pulses ($\pi/2_{mw} = 12$ ns), Fig. 6*F*, and now we see two main features with hyperfine couplings of 28, 35 MHz. No signal is seen with the ^{56}Fe control sample (Fig. 2*G*) under the same conditions. Likewise, no signals are apparent in the low frequency region when using a Mims pulse sequence, ruling out the presence of very small ^{57}Fe hyperfine couplings. Overall, these ^{57}Fe ENDOR results are quite similar to those seen with HMBPP, Fig. 2, and are quite different to those seen in the absence of these ligands, supporting again a direct interaction with the cluster.

Conclusions

In summary, the mechanism we propose is unique in that it involves a novel, bioorganometallic mechanism for IspH catalysis, that is, the formation of transition state/reactive intermediates (π/σ complexes; η^3-allyl complexes) containing metal-carbon bonds, together with the involvement of at least two residues (H124, E126) that deliver H^+ to the active site. The ability of olefins (as well as acetylenes and cyclopentadienides) to bind to $[Fe_4S_4]^+$ (or $[Fe_6Mo_2S_8(SPh)_9]^{3-}$ clusters) is well known in model systems, as well as in the nitrogenase system, and provides precedent for the structures proposed. Of particular importance is the observation that ethylene and allyl alcohol (HMBPP "minus" the Me and $-CH_2OPP$ substituents), form π/σ com-

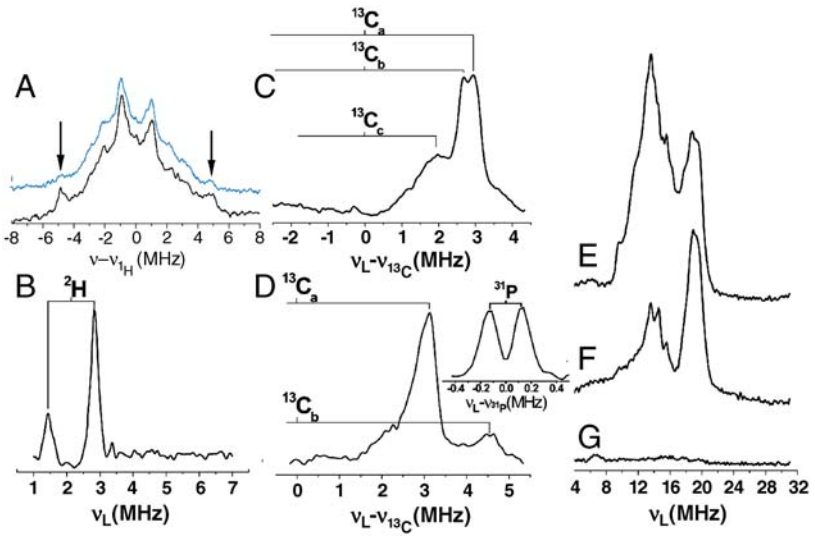

Fig. 6. Alkyne inhibitor ENDOR results. (*A*) IspH + **8**, Davies selective pulse, showing a large ^{1}H hyperfine coupling that is attenuated (*Inset*, *Blue*) in an 80% [3-$^{2}H_1$]-**8** labeled sample. (*B*) IspH + [3-$^{2}H_1$]-**8**, ($^{2}H - ^{1}H$) difference Mims ENDOR spectrum, showing a ^{2}H ENDOR signal with 1.5 MHz coupling. (*C*) IspH + [u-$^{13}C_3$]-**8**, difference Mims ENDOR spectrum showing solely ^{13}C ENDOR. (*D*) IspH + [u-$^{13}C_3$]-**9** difference Mims ENDOR spectrum showing solely ^{13}C ENDOR; the inset shows the ^{31}P Mims ENDOR signals from IspH+ unlabeled **9**. (*E*) [u-^{57}Fe]-IspH + **8**, Davies selective pulse. (*F*) The same as (*E*), but with Davies nonselective pulse. (*G*) Natural abundance ^{57}Fe control, Davies nonselective pulse.

plexes with Fe (in the nitrogenase FeMo cofactor), and similar metallacycles are likely to form (as reactive intermediates or transition states) when HMBPP binds to reduced IspH, with the 4-OH then being ideally poised to be protonated (by E126/H124). This π/σ bonding would not be present with an Fe_3S_4 cluster, which just presents $3S^{2-}$ to the olefin. When compared with previous proposals, the results we have described above differ in several important respects. First, organometallic species (i.e. containing Fe-C bonds) are involved. Second, we find no evidence for stable, carbon-based radicals. Third, there are specific roles for key catalytic residues (in particular, E126). Fourth, the mechanism requires the presence of a fourth, unique Fe. The likely involvement of an η^3 (π) complex (the allyl anion) is also attractive, because other anionic π-complexes, cyclopentadienides, are well known to form π-complexes with Fe_4S_4 clusters. These results are also of broader general interest because they have led to the discovery of the first μM inhibitor of IspH, and based again on EPR, ENDOR, and computational docking results, we propose that these types of inhibitors bind into the IspH active site with their diphosphates occupying the "PPi" site, while their alkyne groups form π/σ complexes with the unique fourth Fe. Overall, these results can be expected to lead to new types of inhibitors of IspH, as well as of other Fe_4S_4 cluster-containing proteins containing "unique" fourth Fe atoms, such as IspG, where again, organometallic species are likely to be involved in catalysis.

Methods

Samples for EPR spectroscopy were reduced either by adding $Na_2S_2O_4$ or by photoreduction in the presence of 5-deazaflavin. EPR spectra were collected at X-band using a Varian E-122 spectrometer together with an Air Products helium cryostat. Data acquisition parameters were typically field center = 3250 G; field sweep = 800 G; modulation = 100 kHz; modulation amplitude = 5 G; time constant = 32 ms; 60 s per scan; 8 s between each scan; and temperature = 15 K. Samples for ENDOR spectroscopy were reduced by adding $Na_2S_2O_4$. Pulsed ENDOR spectra were obtained on a Bruker ElexSys E-580-10 FT-EPR X-band EPR spectrometer using an ENI A 300RF amplifier and an Oxford Instruments CF935 cryostat at 15 K (8 K for unliganded wt [^{57}Fe]-IspH). Davies pulsed ENDOR experiments were carried out for ^{57}Fe samples and the IspH + **8** sample using a three pulse scheme (π_{mw}-*T*-$\pi/2_{mw}$-τ-π_{mw}-τ-echo, π_{rf} applied during *T*) (27) with the excitation field set to correspond to g_2. ^{57}Fe Davies ENDOR spectra were collected with either $\pi/2_{mw}$ = 12 ns (nonselective) or $\pi/2_{mw}$ = 48 ns (selective) pulse excitation. The selective pulse scheme was also used for acquiring ^{1}H ENDOR spectra of IspH + **8**. For other samples, Mims pulsed ENDOR with a three pulse scheme ($\pi/2_{mw}$-τ-$\pi/2_{mw}$-*T*-$\pi/2_{mw}$-τ-echo, $\pi/2_{mw}$ = 16 ns, and π_{RF} applied during *T*) (27) was used, with the excitation field set to correspond to g_2. τ-averaging (32 spectra at 8 ns step) was used to reduce the blind spots that arise from the τ-dependent oscillations.

Further details of site-directed mutagenesis, protein purification and reconstitution, enzymatic assays, computational aspects, and compound synthesis are reported in *SI Text, Supplementary Methods*.

ACKNOWLEDGMENTS. We thank Pinghua Liu for providing his *E. coli* IspG plasmid, Hassan Jomaa, and Jochen Wiesner for providing their *A. aeolicus* IspH plasmid, and Thomas B. Rauchfuss and a reviewer, for helpful suggestions. This work was supported by the United States Public Health Service (NIH Grants GM65307 and GM073216).

1. Rohmer M, Grosdemange-Billiard C, Seemann M, Tritsch D (2004) Isoprenoid biosynthesis as a novel target for antibacterial and antiparasitic drugs. *Curr Opin Invest Dr* 5:154–162.
2. Martin MB, Arnold W, Heath HT, III, Urbina JA, Oldfield E (1999) Nitrogen-containing bisphosphonates as carbocation transition state analogs for isoprenoid biosynthesis. *Biochem Biophys Res Commun* 263:754–758.
3. Guo RT, et al. (2007) Bisphosphonates target multiple sites in both *cis*- and *trans*-prenyltransferases. *Proc Natl Acad Sci USA* 104:10022–10027.
4. Rodriguez N, et al. (2002) Radical cure of experimental cutaneous leishmaniasis by the bisphosphonate pamidronate. *J Infect Dis* 186:138–140.
5. Benaim G, et al. (2006) Amiodarone has intrinsic anti-*Trypanosoma cruzi* activity and acts synergistically with posaconazole. *J Med Chem* 49:892–899.
6. Paniz-Mondolfi AE, Perez-Alvarez AM, Lanza G, Marquez E, Concepcion JL (2009) Amiodarone and itraconazole: A rational therapeutic approach for the treatment of chronic Chagas' disease. *Chemotherapy* 55:228–233.
7. Paniz-Mondolfi AE, et al. (2008) Concurrent Chagas' disease and borderline disseminated cutaneous leishmaniasis: The role of amiodarone as an antitrypanosomatidae drug. *Ther Clin Risk Manag* 4:659–663.
8. Zhang Y, et al. (2009) Lipophilic bisphosphonates as dual farnesyl/geranylgeranyl diphosphate synthase inhibitors: An x-ray and NMR investigation. *J Am Chem Soc* 131:5153–5162.
9. Liu CI, et al. (2008) A cholesterol biosynthesis inhibitor blocks *Staphylococcus aureus* virulence. *Science* 319:1391–1394.
10. Borrmann S, et al. (2006) Fosmidomycin plus clindamycin for treatment of pediatric patients aged 1 to 14 years with *Plasmodium falciparum* malaria. *Antimicrob Agents Ch* 50:2713–2718.
11. Rohmer M (2008) From molecular fossils of nacterial hopanoids to the formation of isoprene units: Discovery and elucidation of the methylerythritol phosphate pathway. *Lipids* 43:1095–1107.
12. Rekittke I, et al. (2008) Structure of (E)-4-hydroxy-3-methyl-but-2-enyl diphosphate reductase, the terminal enzyme of the non-mevalonate pathway. *J Am Chem Soc* 130:17206–17207.
13. Gräwert T, et al. (2009) Structure of active IspH enzyme from *Escherichia coli* provides mechanistic insights into substrate reduction. *Angew Chem Int Ed Engl* 48:5756–5759.
14. Gräwert T, et al. (2004) IspH protein of *Escherichia coli*: Studies on iron-sulfur cluster implementation and catalysis. *J Am Chem Soc* 126:12847–12855.
15. Wolff M, et al. (2003) Isoprenoid biosynthesis via the methylerythritol phosphate pathway: The (E)-4-hydroxy-3-methylbut-2-enyl diphosphate reductase (LytB/IspH) from *Escherichia coli* is a [4Fe-4S] protein. *FEBS Lett* 541:115–120.
16. Seemann M, et al. (2009) Isoprenoid Biosynthesis via the MEP Pathway: In vivo Mössbauer spectroscopy identifies a $[4Fe\text{-}4S]^{2+}$ center with unusual coordination sphere in the LytB protein. *J Am Chem Soc* 131:13184–13185.
17. Xiao Y, Chu L, Sanakis Y, Liu P (2009) Revisiting the IspH catalytic system in the deoxyxylulose phosphate pathway: Achieving high activity. *J Am Chem Soc* 131:9931–9933.
18. Altincicek B, et al. (2002) LytB protein catalyzes the terminal step of the 2- *C*-methyl-D-erythritol-4-phosphate pathway of isoprenoid biosynthesis. *FEBS Lett* 532:437–440.
19. Rohdich F, et al. (2003) The deoxyxylulose phosphate pathway of isoprenoid biosynthesis: Studies on the mechanisms of the reactions catalyzed by IspG and IspH protein. *Proc Natl Acad Sci USA* 100:1586–1591.
20. Xiao Y, Zhao ZK, Liu P (2008) Mechanistic studies of IspH in the deoxyxylulose phosphate pathway: Heterolytic C-O bond cleavage at C_4 position. *J Am Chem Soc* 130:2164–2165.
21. Xiao Y, Liu P (2008) IspH protein of the deoxyxylulose phosphate pathway: Mechanistic studies with C_1-deuterium-labeled substrate and fluorinated analogue. *Angew Chem Int Ed Engl* 47:9722–9725.
22. Lee HI, et al. (2004) An organometallic intermediate during alkyne reduction by nitrogenase. *J Am Chem Soc* 126:9563–9569.
23. Pelmenschikov V, Case DA, Noodleman L (2008) Ligand-bound $S = 1/2$ FeMo-cofactor of nitrogenase: Hyperfine interaction analysis and implication for the central ligand X identity. *Inorg Chem* 47:6162–6172.
24. Lee HI, et al. (2005) Electron inventory, kinetic assignment (E_n), structure, and bonding of nitrogenase turnover intermediates with C_2H_2 and CO. *J Am Chem Soc* 127:15880–15890.
25. Friesner RA, et al. (2006) Extra precision glide: Docking and scoring incorporating a model of hydrophobic enclosure for protein-ligand complexes. *J Med Chem* 49:6177–6196.
26. Tanaka K, Nakamoto M, Tsunomori M, Tanaka T (1987) Raman-spectra of the adducts of reduced species of $[Fe_4S_4(SPh)_4]^{2-}$ and $[Mo_2Fe_6S_8(SPh)_9]^{3-}$ with acetylene. *Chem Lett* 613–616.
27. Gemperle C, Schweiger A (1991) Pulsed electron nuclear double-resonance methodology. *Chem Rev* 91:1481–1505.
28. Perera SA, Salemi LM, Bartlett RJ (1996) Hyperfine coupling constants of organic radicals. *J Chem Phys* 106:4061.
29. Schunn RA, Fritchie CJ, Jr, Prewitt CT (1966) Syntheses of some cyclopentadienyl transition metal sulfides and the crystal structure of $(C_5H_5FeS)_4$. *Inorg Chem* 5:892–899.
30. McMillan RS, Renaud J, Reynolds JG, Holm RH (1979) Biologically related iron-sulfur clusters as reaction centers. Reduction of acetylene to ethylene in systems based on $[Fe_4S_4(SR)_4]^{3-}$. *J Inorg Biochem* 11:213–227.
31. Itoh T, Nagano T, Hirobe M (1980) $[Fe_4S_4(SR)_4]^{2-}$ Catalytic reduction of diphenylacetylene to *cis*-stilbene in the presence of $NaBH_4$. *Tetrahedron Lett* 21:1343–1346.
32. Millen RP, de Faria DLA, Temperini MLA (2001) Vibrational spectra of 2-ethynylpyridine and its silver salt. *Vib Spectrosc* 27:89–96.